

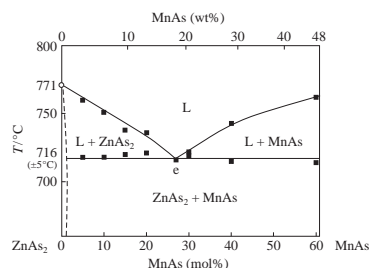
## Phase diagram of ZnAs<sub>2</sub>–MnAs system

 Sergey F. Marenkin,<sup>a,b</sup> Alexey I. Ril'skiy<sup>a</sup> and Irina V. Fedorchenko<sup>a,b</sup>
<sup>a</sup> N. S. Kurnakov Institute of General and Inorganic Chemistry, Russian Academy of Sciences, 119991 Moscow, Russian Federation. E-mail: lelrik101@mail.ru

<sup>b</sup> National University of Science and Technology 'MISIS', 119049 Moscow, Russian Federation

DOI: 10.1016/j.mencom.2018.03.038

The ZnAs<sub>2</sub>–MnAs system, characterized by X-ray powder diffraction, differential thermal and microstructure studies, is of the eutectic type, with the coordinates of eutectic 73 mol% ZnAs<sub>2</sub> and 27 mol% MnAs and  $T_m = 716^\circ\text{C}$ . The solubility of MnAs in ZnAs<sub>2</sub> is lower 1 mol%. Alloys of ZnAs<sub>2</sub> with MnAs are ferromagnetic with  $T_c \approx 318\text{ K}$ , their magnetization being increased with raising the MnAs content.



In parallel with the design of new spintronic materials based on superlattices formed as a combination of magnetic and non-magnetic nanolayers, in which giant magnetic resistance (GMR)<sup>1–3</sup> and tunnel magnetic resistance (TMR)<sup>4,5</sup> effects were discovered, an intense research is now underway into grained structures comprised of a nonmagnetic matrix and ferromagnetic nano-inclusions.<sup>6</sup> The matrix can be nonmagnetic metals<sup>7–9</sup> or insulators.<sup>10</sup> Our standpoint is that semiconductor matrix shows the greatest promise in this context.<sup>11–13</sup> Semiconductors are distinguished by high carrier motility, long relaxation times, and thereby considerable free paths of carriers. This facilitates the design of grained structures with GMR and TMR effects.

The semiconductor matrix we chose to use in this study was ZnAs<sub>2</sub> and ferromagnetic component was MnAs. ZnAs<sub>2</sub> is a hopping semiconductor with a band gap of 1 eV and considerable anisotropic optical and electric properties. It crystallizes in the monoclinic structure (space group  $P2_1/c$ ) with the unit cell parameters:  $a = 9.277$ ,  $b = 7.691$  and  $c = 8.010\text{ \AA}$ .<sup>14,15</sup> MnAs is a ferromagnetic with the Curie point at 318 K and with saturation magnetization of 3.4  $\mu\text{B}$  per manganese atom,<sup>16</sup> which has semi-metal properties and 300 K conductivity of  $\sim 2 \times 10^4\ \Omega\ \text{cm}^{-1}$ .<sup>17</sup>

The ferromagnetic MnAs phase crystallizes in hexagonal lattice (space group  $P6_3/mmc$ ) with the unit cell parameters  $a = 3.72$  and  $c = 5.71\text{ \AA}$  and transforms into a paramagnetic phase at 40–45°C, which crystallizes in an orthorhombic lattice (space group  $Pnma$ ).<sup>18,19</sup>

To choose optimal compositions and synthesis parameters for grained structures, phase equilibrium in the ZnAs<sub>2</sub>–MnAs system was studied using a set of physicochemical methods.<sup>†</sup>

XRD pattern of precursors (Figure 1, curves 1, 4) coincided with the ICDD PDF-2 for ZnAs<sub>2</sub> and MnAs.<sup>11,16</sup> The synthesized precursors crystallized in the space group  $P2_1/c$  for ZnAs<sub>2</sub> and space group  $P6_3/mmc$  for MnAs. The corresponding XRD patterns

<sup>†</sup> The alloys of ZnAs<sub>2</sub> and MnAs were obtained from the compounds synthesized by the fusion of the high-purity elements Zn, As and Mn. The synthesis was carried out in electric furnaces using temperature regulators, with accuracy of  $\pm 1$  and computer control in double walled fused silica ampoules evacuated to  $\sim 2\text{--}10\text{ Pa}$ . The inner ampoule was graphitized to exclude the reaction of its walls with melts. The temperature and time regimes were chosen in view of high arsenic vapor pressures. First, the sample was heated up to 630°C and incubated at this temperature for at least 24 h. The long time of exposure served for better homogenization. The second step involved heating at 20 K h<sup>-1</sup> up to 930°C and subsequent exposure for a period of up to 24 h for homogenization of melt. The mass of each sample was  $\sim 10\text{ g}$ .

The samples were investigated by X-ray powder diffraction (XRD), differential thermal analysis (DTA), optical and scanning electron microscopy (SEM). XRD experiments were performed on a Bruker D8 Advance instrument (CuK $\alpha$  radiation,  $\lambda = 0.1540\text{ nm}$ ,  $U = 40\text{ kV}$ ,  $I = 40\text{ mA}$ ). The recording parameters were 0.005° per 2 s of exposure in the range  $10^\circ \leq 2\theta \leq 90^\circ$ . The X-ray diffraction patterns were processed with reference to the ICDD PDF-2 powder. Microstructures were analyzed with the EPIQUANT optical metallographic microscope and the Carl Zeiss N Vision 40 scanning electron microscope equipped with Oxford Instruments X-Max analyzer. Quantitative composition was calculated from the recorded energy spectrum of the emitted X-radiation. The samples preparation for the microstructure included cutting ingots to the washers, grinding by powder SiC with the 20  $\mu\text{m}$  granularity, and polishing with the diamond paste with the 1  $\mu\text{m}$  granularity. The etching of samples in the dilute solution of nitric acid or CP4 (HNO<sub>3</sub>–HF–AcOH, 5:3:3) with the subsequent washing in the ultrasonic bath for optical studies was carried out.

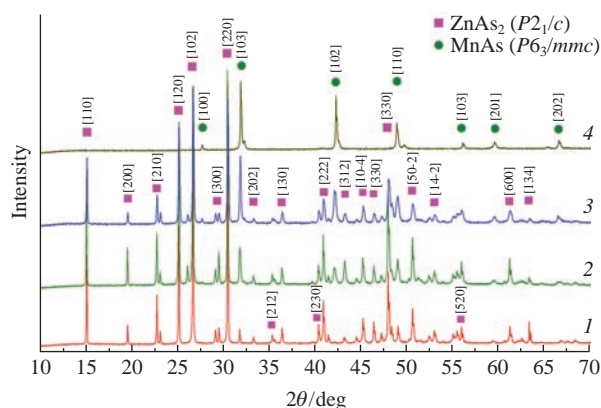


**Figure 1** X-ray diffraction patterns: (1) ZnAs<sub>2</sub> precursor, (2) 80 mol% ZnAs<sub>2</sub> and 20 mol% MnAs, (3) 60 mol% ZnAs<sub>2</sub> and 40 mol% MnAs, (4) MnAs precursor.

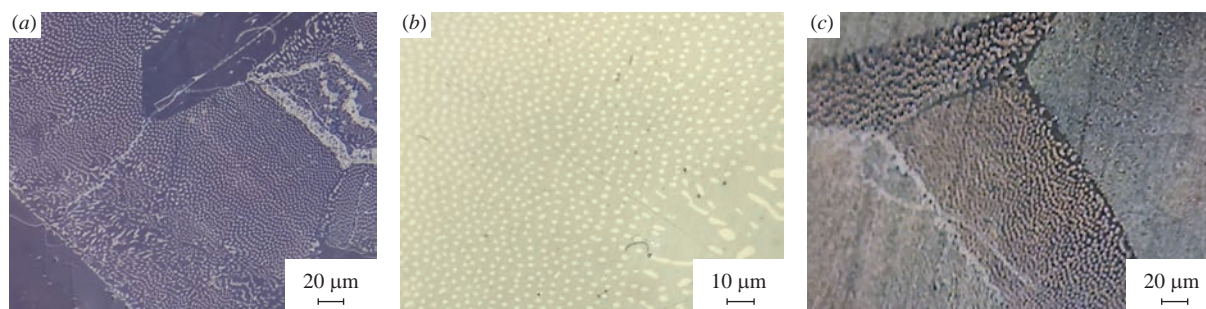


**Figure 2** Microstructure of alloys (a) 90 mol% ZnAs<sub>2</sub> and 10 mol% MnAs, (b) 73 mol% ZnAs<sub>2</sub> and 27 mol% MnAs (eutectic), (c) 40 mol% ZnAs<sub>2</sub> and 60 mol% MnAs.

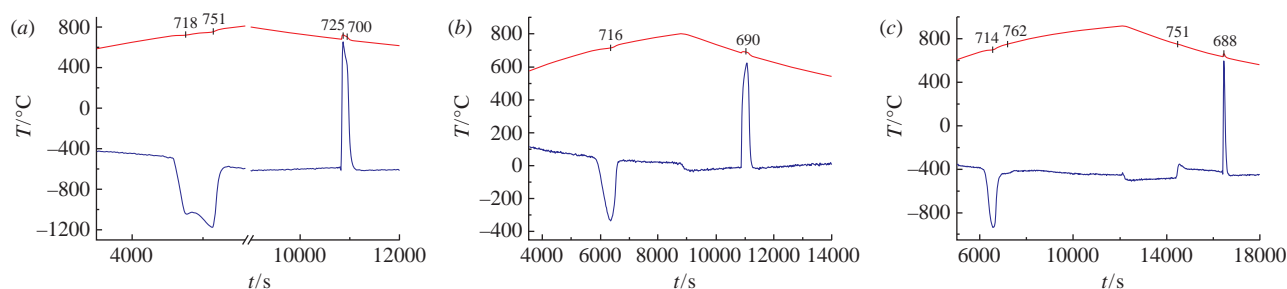


**Figure 3** DTA curves of alloys (a) 90 mol% ZnAs<sub>2</sub> and 10 mol% MnAs, (b) 73 mol% ZnAs<sub>2</sub> and 27 mol% MnAs, (c) 40 mol% ZnAs<sub>2</sub> and 60 mol% MnAs.

of alloys (Figure 1, curves 2, 3) contained the peaks which relate only to the phases ZnAs<sub>2</sub> and MnAs. The change in the position of peaks ZnAs<sub>2</sub> in the alloys was insignificant. Parameters of the unit cell for ZnAs<sub>2</sub> in alloys are somewhat increased ( $a = 9.2891$ ,  $b = 7.6890$  and  $c = 8.091$  Å) as compared with those for pure ZnAs<sub>2</sub> ( $a = 9.277$ ,  $b = 7.691$  and  $c = 8.010$  Å),<sup>14</sup> which indicated the small solubility of MnAs.

According to the microstructure analysis, ZnAs<sub>2</sub> and MnAs form an eutectic system. All alloys contain two phases: phase ZnAs<sub>2</sub> and eutectic [Figure 2(a)], eutectic [Figure 2(b)], phase MnAs and eutectic [Figure 2(c)]. The composition of eutectic was determined by SEM: for MnAs phase, 49.1 at% (Mn), and 49.1 at% (As); for ZnAs<sub>2</sub> phase, 0.9 at% (Mn), 32.1 at% (Zn) and 66.2 at% (As). These data show the solubility of Mn in ZnAs<sub>2</sub> ~1 at%.

DTA data correlate with the results of X-ray and microstructure analysis (Figure 3). According to the DTA of the alloy 90 and 10 mol% MnAs, the heating cycle has endothermic effect at 718 and 751 °C, which appears to be the effect of melting eutectic and the liquids from the side ZnAs<sub>2</sub>, respectively.

The DTA showed these effects in cooling cycle at 700 and 725 °C [Figure 3(a)]. The significant super cooling upon the crystallization is characteristic of the polyanion semiconductors, ZnAs<sub>2</sub> relates to this category. Such semiconductors have connections metal–anion (zinc–arsenic) and anion–anion (arsenic–arsenic).

According to the DTA of heating and cooling cycles, the alloy 73 mol% ZnAs<sub>2</sub> and 27 mol% MnAs relates to eutectic composition [Figure 3(b)]. The DTA of heating cycle had one endothermic effect at 716 °C (eutectic point). Such an effect occurred at 690 °C in the DTA of cooling cycle. The DTA of heating and cooling cycles of the alloy 40 and 60 mol% is shown in Figure 3(c). According to microstructure this alloy appeared after the eutectic

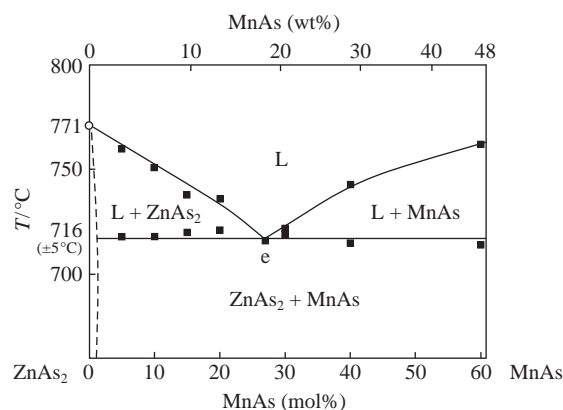


**Figure 4** The phase diagram of ZnAs<sub>2</sub>–MnAs system. L is the liquid.

composition. Two endothermic effects occurred at 714 and 762 °C in the DTA of heating cycle. The first effect corresponded to the melting eutectic, the second effect related to the liquid MnAs. These effects in the cooling cycle were observed at 688 and 751 °C of DTA curve. The decrease in the value of super cooling upon the increase in MnAs concentrations emphasizes the determining role of the ZnAs<sub>2</sub> phase.

The phase diagram of ZnAs<sub>2</sub>–MnAs system was constructed based on the DTA, X-ray and SEM data (Figure 4). The coordinates of eutectic are 73 mol% ZnAs<sub>2</sub> and 27 mol% MnAs with  $T_{\text{melt}} = 716$  °C.

The alloys of ZnAs<sub>2</sub> with MnAs were ferromagnetic, with  $T_c$  of ~318 K. The magnetization of these alloys increased if the MnAs content was higher.

In conclusion, ZnAs<sub>2</sub>–MnAs is a quasi-binary section of the Zn–As–Mn system. The interaction of ZnAs<sub>2</sub> and MnAs has eutectic character. The alloys of zinc diarsenide with manganese arsenide are ferromagnetic. The magnetization of these alloys enlarges with the increase in the MnAs content.

This work was supported by the Russian Foundation for Basic Research (grant no. 16-03-00796) and the Ministry of Education and Science of the Russian Federation in the framework of Increase Competitiveness Programme of MISIS (P02-2017-1-16).

Phase transition temperatures were obtained from DTA measurements. DTA was performed using 90% Pt with 10% Re as the thermocouples calibrated according to the melting points of the high-purity elements Sn, Zn, Sb, Al, Ge. The heating rate was 5 K min<sup>-1</sup>. The accuracy of the determination of the temperature of thermal effects was ±5 K. The measurements were made in evacuated and sealed quartz Stepanov's vessels. The weight of models was 1.5 g.

## References

- 1 M. N. Baibich, J. M. Broto, A. Fert, F. N. Van Dau, F. Petroff, P. Etienne, G. Creuzet, A. Friederich and J. Chazelas, *Phys. Rev. Lett.*, 1988, **61**, 2472.
- 2 A. E. Berkowitz, J. R. Mitchell, M. J. Carey, A. P. Young, S. Zhang, F. E. Spada, F. T. Parker, A. Hutten and G. Thomas, *Phys. Rev. Lett.*, 1992, **68**, 3745.
- 3 C. L. Chien, J. Q. Xiao and J. S. Jiang, *J. Appl. Phys.*, 1993, **73**, 5309.
- 4 T. Miyazaki and N. Tezuka, *J. Magn. Magn. Mater.*, 1995, **151**, 403.
- 5 S. S. P. Parkin, C. Kaiser, A. Panchula, P. M. Rice, B. Hughes, M. Samant and S.-H. Yang, *Nat. Mater.*, 2004, **3**, 862.
- 6 S. A. Gridnev, Yu. E. Kalinin, A. V. Sitnikov and O. V. Stogney, *Nelineinye yavleniya v nano- i mikroheterogennykh sistemakh (Nonlinear Phenomena in Nano- and Micro-Heterogeneous Systems)*, BINOM, Moscow, 2012 (in Russian).
- 7 A. V. Ognev and A. S. Samardak, *Vestn. DVO RAN*, 2006, **4**, 70 (in Russian).
- 8 A. Yu. Soloveva, Yu. V. Ioni and S. P. Gubin, *Mendeleev Commun.*, 2016, **26**, 38.
- 9 Yu. G. Khabarov, I. M. Babkin, N. Yu. Kuzyakov, V. A. Veshnyakov, V. A. Plakhin, A. S. Orlov, D. G. Chukhchin and E. A. Varakin, *Mendeleev Commun.*, 2017, **27**, 186.
- 10 A. E. Berkowitz, J. R. Mitchell, M. J. Carey, A. P. Young, S. Zhang, F. E. Spada, F. T. Parker, A. Hutten and G. Thomas, *Phys. Rev. Lett.*, 1992, **68**, 3745.
- 11 B. A. Aronzon, A. A. Likalter, V. V. Rylkov, A. K. Sarychev, M. A. Sedova and A. E. Varfolomeev, *Phys. Status Solidi B*, 1998, **205**, 151.
- 12 I. V. Fedorchenko, A. V. Kochura, S. F. Marenkin, A. N. Aronov, L. I. Koroleva, L. Kilanski, R. Szymczak, W. Dobrowolski, S. Ivanenko and E. Lähderanta, *IEEE Trans. Magn.*, 2012, **48**, 1581.
- 13 S. F. Marenkin, A. D. Izotov, I. V. Fedorchenko and V. M. Novotortsev, *Russ. J. Inorg. Chem.*, 2015, **60**, 295 (*Zh. Neorg. Khim.*, 2015, **60**, 343).
- 14 V. G. Yarzhemsky, S. V. Murashov, V. I. Nefedov and E. N. Muraviev, *Inorg. Mater.*, 2008, **44**, 1169 (*Neorg. Mater.*, 2008, **44**, 1300).
- 15 M. E. Fleet, *Acta Crystallogr., Sect. B*, 1974, **30**, 122.
- 16 W. J. Turner, A. S. Fischler and W. E. Reese, *Phys. Rev.*, 1961, **121**, 759.
- 17 G. A. Govor, *Phys. Solid State*, 2015, **57**, 871 (*Fiz. Tverd. Tela*, 2015, **57**, 857).
- 18 G. Fischer and W. B. Pearson, *Can. J. Phys.*, 1958, **36**, 1010.
- 19 H. Okamoto, *Bull. Alloy Phase Diagrams*, 1989, **10**, 549.

Received: 24th August 2017; Com. 17/5337